

# Compartmentalization and Photoregulating Pathways for Incompatible Tandem Catalysis

Peiyuan Qu, Michael Kuepfert, Maryam Hashmi, and Marcus Weck\*



Cite This: *J. Am. Chem. Soc.* 2021, 143, 4705–4713



Read Online

ACCESS |



Metrics & More

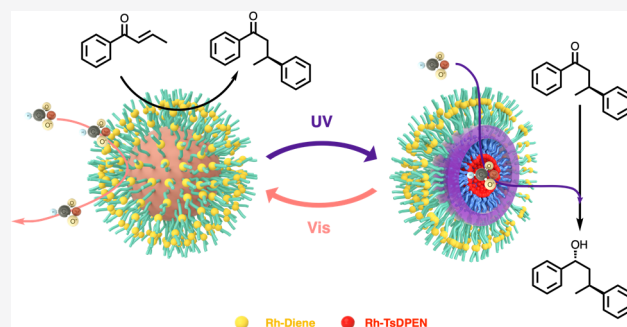


Article Recommendations



Supporting Information

**ABSTRACT:** This contribution describes an advanced compartmentalized micellar nanoreactor that possesses a reversible photoresponsive feature and its application toward photoregulating reaction pathways for incompatible tandem catalysis under aqueous conditions. The smart nanoreactor is based on multifunctional amphiphilic poly(2-oxazoline)s and covalently cross-linked with spiropyran upon micelle formation in water. It responds to light irradiation in a wavelength-selective manner switching its morphology as confirmed by dynamic light scattering and cryo-transition electron microscopy. The compartmental structure renders distinct nanoconfinements for two incompatible enantioselective transformations: a rhodium–diene complex-catalyzed asymmetric 1,4-addition occurs in the hydrophilic corona, while a Rh-TsDPEN-catalyzed asymmetric transfer hydrogenation proceeds in the hydrophobic core. Control experiments and kinetic studies showed that the gated behavior induced by the phototriggered reversible spiropyran to merocyanine transition in the cross-linking layer is key to discriminate among substrates/reagents during the catalysis. The smart nanoreactor realized photoregulation to direct the reaction pathway to give a multichiral product with high conversions and perfect enantioselectivities in aqueous media. Our SCM catalytic system, on a basic level, mimics the concepts of compartmentalization and responsiveness Nature uses to coordinate thousands of incompatible chemical transformations into streamlined metabolic processes.



## INTRODUCTION

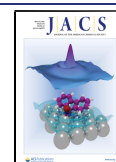
Multistep synthesis via a one-pot procedure is of great importance in modern organic synthesis due to economic and environmental considerations.<sup>1–4</sup> It often involves two or more chemical transformations that are carried out in a single reaction vessel and mediated by multiple catalysts. Combining multiple discrete catalysts in a single reaction vessel generally engenders catalyst deactivation.<sup>5</sup> Additionally, successful execution of a multistep synthesis relies on programming the reaction sequence as well as controlling selectivity between multiple competitive reaction pathways since undesired pathways will lead to side products and lower yields.<sup>6</sup> The fundamental design strategies of Nature overcome such catalyst incompatibility and reaction sequencing by positionally assembling active species inside subcellular compartments, separated by membranes.<sup>7–9</sup> The cell performs metabolic processes via the most efficient pathway by tuning membrane permeability in response to regulatory signals, which governs the transportation of molecules for catalysis and orchestrates thousands of incompatible transformations into a streamlined biosynthetic route.<sup>10,11</sup>

Scientists have developed multicompartamental catalytic systems based on various strategies including the use of sol-gels,<sup>12</sup> Pickering emulsion droplets,<sup>13</sup> supramolecular metal complex architectures,<sup>14,15</sup> and polymers.<sup>16,17</sup> Catalytic frame-

works fabricated from these materials have realized compartmentalization for multiple active catalytic sites, as epitomized by the cell, and enabled multistep nonorthogonal transformations.<sup>12–14,18–23</sup> Incorporating responsive elements into the support structures has rendered them “smart”, i.e., allowing for reversible alterations of the physical and chemical properties in response to external stimuli such as temperature,<sup>24,25</sup> pH,<sup>26</sup> light,<sup>27,28</sup> or enzymes.<sup>29,30</sup> The properties of the resulting smart materials impart an additional bioinspired control over single-step catalytic transformations.<sup>24,31–35</sup> Manipulation of multicatalytic tandem sequences, however, remains challenging and restricted to the regulation of reactivities via temperature actuation.<sup>36,37</sup> This limitation significantly affects the choice of catalysts and limits the feasibility of performing one-pot tandem catalysis at arbitrary temperature ranges. To date, no “smart” catalytic system can use or control different switchable states to tune and activate a

Received: January 8, 2021

Published: March 16, 2021



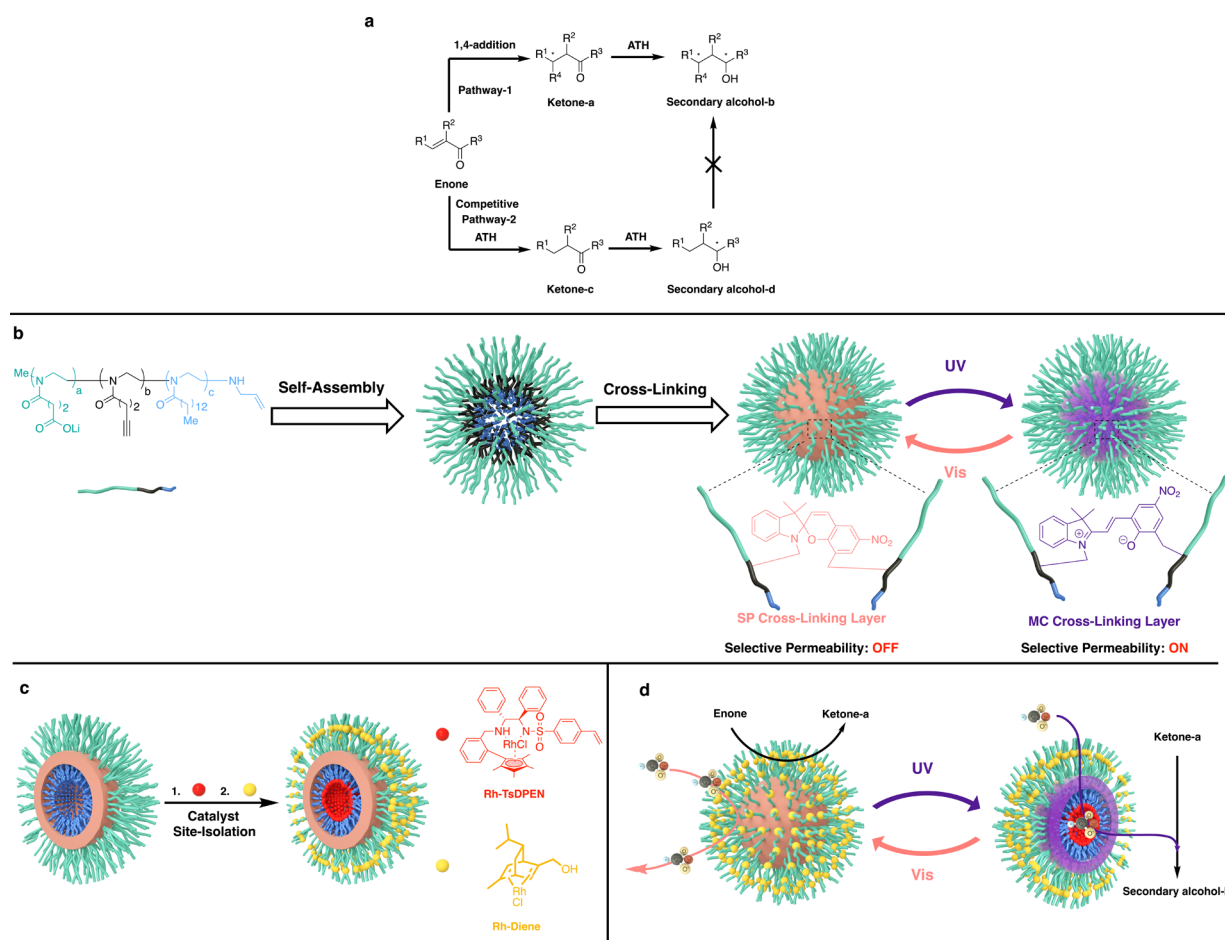


**Figure 1.** Rational design of “smart” SCMs nanoreactors for photoregulating incompatible tandem catalysis. (a) Targeted two-step tandem catalysis, Pathway-1, to synthesize the secondary alcohol-b from an enone. The competitive pathway, Pathway-2, generates ketone-c and the secondary alcohol-d. (b) Design and structural motifs of the polymeric scaffold: assembly of amphiphilic ABC-triblock copolymers with orthogonal functional groups at various locations into core–shell micelles followed by the cross-linking with spiropyran (SP) to yield the target SCM. Reversible photochromism between SP-SCM and the zwitterionic merocyanine (MC)-SCM form accompanied by switchable permeability of the micelle shell. (c) Compartmentalization of two incompatible metal catalysts in distinct microenvironments (hydrophobic core and hydrophilic shell) on the SCM support. (d) Access to microenvironments can be phototriggered enabling molecular discrimination and suppression of competitive steps.

desired synthetic pathway among many possible ones during a multistep synthesis.

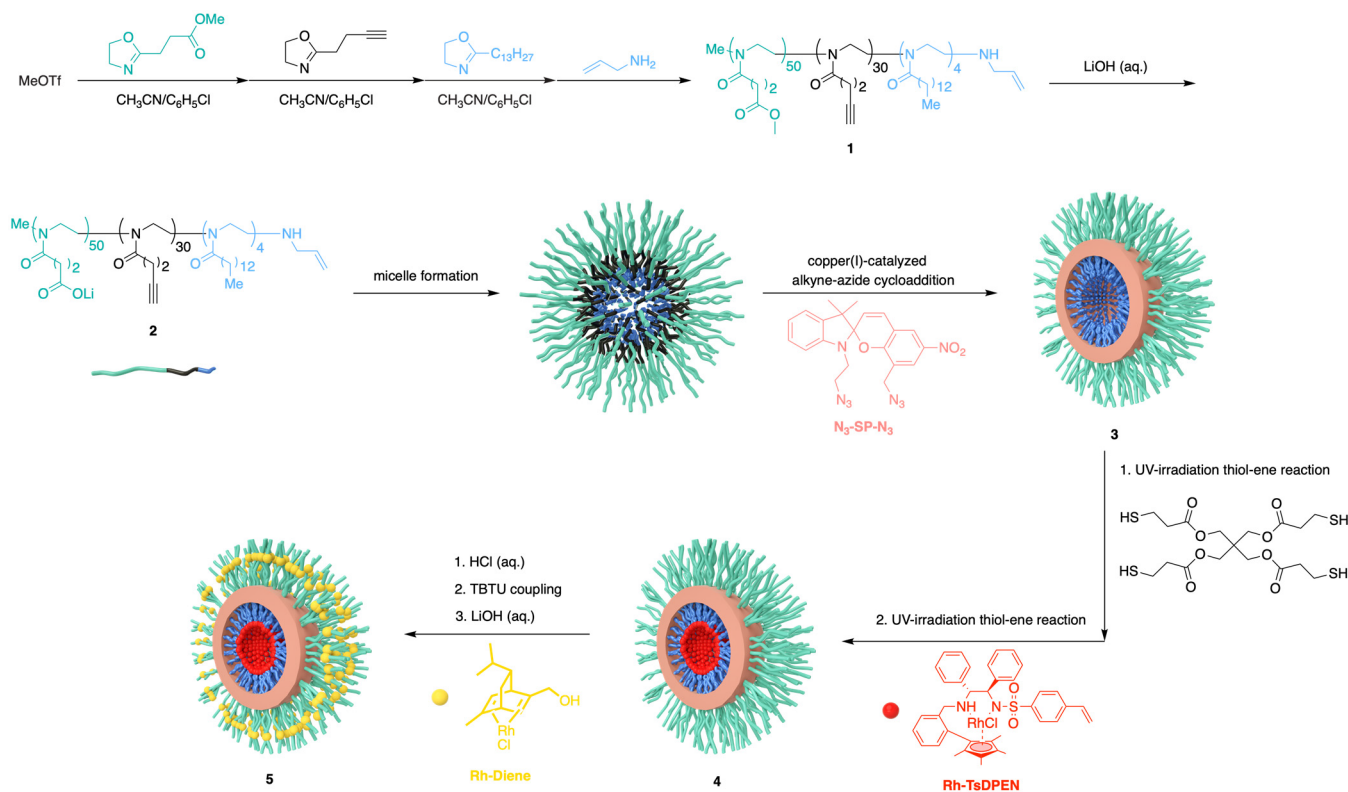
Among artificial materials, polymers have attracted increasing attention as catalyst supports, such as polymersomes for multistep enzymatic cascade catalysis<sup>38–40</sup> and star polymers for acid–base tandem catalysis.<sup>41,42</sup> In particular, shell cross-linked micelles (SCMs) are an attractive scaffold for supported catalysis due to their robustness, tenability, and potential for functionalization in multiple domains.<sup>43</sup> The unique hydrophobic pocket and the intramicellar diffusion of substrates within the nanostructure can facilitate tandem catalysis in aqueous media.<sup>44–46</sup> We have used SCMs as compartmentalized nanoreactors for nonorthogonal tandem catalysis.<sup>45–48</sup> To realize a cell-like microenvironment for catalysis, the incorporation of both compartmentalization and responsiveness into a single support structure is key. By engineering responsive units within traditional SCMs, we take a significant step toward this goal. Herein, we report such a “smart” catalytic system that includes a morphology switch to realize orthogonal modulation of different catalysts/catalytic processes. Our photoresponsive SCM nanoreactor operates in water and is designed for two nonorthogonal enantioselective

transformations: the Rh–diene-catalyzed asymmetric 1,4-addition of enones and the rhodium-N-tosylated 1,2-diphenyl-1,2-ethylenediamine (Rh-TsDPEN) catalyzed asymmetric transfer hydrogenation (ATH). Light exposure directs the tandem catalysis toward the desired reaction pathway and results in a diastereomeric product with excellent conversions and stereoselectivities.

## RESULTS AND DISCUSSION

The primary target of our tandem catalysis is to synthesize the secondary alcohol-b with two chiral centers (Figure 1a). The Rh-catalyzed 1,4-addition of arylboronic acids to commercially available enones was used to form the corresponding  $\beta$ -arylated carbonyl compounds that were subsequently transformed by the Rh-catalyzed ATH into the chiral secondary alcohols. Rhodium–chiral diene complexes have been reported to efficiently catalyze the asymmetric 1,4-addition of enones to the corresponding  $\beta$ -arylated carbonyl compounds with excellent yields and enantioselectivities under mild reaction conditions.<sup>49,50</sup> ATH mediated by transition-metal complexes with N-tosylated 1,2-diphenyl-1,2-ethylenediamine (TsDPEN) derivatives as ligands is a powerful method to prepare

Scheme 1. Fabrication of Smart SCM Nanoreactors



enantioenriched chiral alcohols from ketones.<sup>51–53</sup> In one pot, both catalytic transformations proceed simultaneously from the onset and cannot be orchestrated into a proper sequence of events (Figure 1a). As a result, the native reactivity profile of the tandem catalysis has two reaction pathways that are mutually competitive, which is not conducive to generate the desired product in high yields. The intermediates and the final product secondary alcohol-d from the competitive pathway are side products and complicate the desired product isolation. Our strategy is to compartmentalize the two incompatible catalysts to avoid mutual interference between multiple transformations and to photoregulate and ultimately direct the tandem catalysis toward the desired reaction pathway.

A critical design element of the smart SCM nanoreactor is the introduction of multiple orthogonal functionalities at various locations on the polymer scaffold, e.g., the side chains and the termini of the main chain (Figure 1b). The straightforward yet efficient self-assembly of well-defined amphiphilic block copolymers in selective solvents enables a high degree of control over morphology and the positions of multifold functions throughout three dimensions, which is pivotal for precisely cross-linking the micelles or attaching catalysts.<sup>43</sup> Covalent cross-linking of dynamic micellar structures affords stable self-assembled nanostructures.<sup>43</sup> Spiropyran (SP), a photochromic molecule,<sup>54,55</sup> was used to covalently cross-link the micelles. Light is chosen as the external trigger due to its facile operation, noninvasiveness, and precise spatiotemporal control. Spiropyran responds to light irradiation in a wavelength-selective manner and reversibly isomerizes between the hydrophobic SP form and the hydrophilic zwitterionic merocyanine (MC). We hypothesized that this SP to MC photochromic transition can be translated into the cross-linking layer leading to a light-induced gating

behavior of the shell accompanied by tunable permeability (Figure 1b).

The chiral rhodium diene complex was immobilized in the hydrophilic corona, while the Rh-TsDPEN catalyst was sequestered into the hydrophobic core (Figure 1c). This spatial arrangement implements nature's fundamental compartmentalization principles to site-isolate active catalytic sites. For aqueous-based tandem catalysis, the diffusion of hydrophobic substrates from the aqueous bulk solution into the core is a major driving force for conversion inside micellar nanoreactors.<sup>44,48</sup> Therefore, the spatial positioning of each catalyst inside the SCM nanoreactor corresponds to the diffusion pathway. Rh–diene complex-catalyzed asymmetric 1,4-addition of arylboronic acids to enones was reported with water as the best solvent,<sup>50</sup> and thus, the hydrophilic corona serves as a preferred nanodomain for immobilization of the chiral Rh–diene complexes.

Rh-TsDPEN is anchored in the micelle core surrounded by a photoswitchable shell. The gating behavior of the micellar shell provides a spatiotemporal modulation of mass transport and regulates the catalysis of the ATH. Prior to UV exposure, the hydrophobic SP cross-linked layer prevents the water-soluble HCOONa, the hydrogen donor, from diffusing into the core, thereby suppressing ATH catalysis. Upon UV light irradiation, the phototriggered transition from SP to MC increases the permeability of the shell and enables the diffusion of HCOONa between compartments to continue the tandem catalysis (Figure 1d).

The SCM nanoreactor was formed from the assembly of amphiphilic poly(2-oxazoline)-based ABC-triblock copolymers (Scheme 1). By using functional initiators, monomers, and terminators, poly(2-oxazoline)s with high functionality fidelity can be synthesized through living cationic ring-opening

polymerization (CROP).<sup>56–58</sup> The triblock copolymers are comprised of a carboxylic acid salt-based hydrophilic block, a cross-linkable middle block containing a terminal alkyne, and a hydrophobic block containing an alkyl tail and a terminal allylamine as the functional handle for postpolymerization modification in the micellar core. The carboxylic acid salts can be transformed into the corresponding carboxylic acids providing a functional handle for the attachment of the hydroxy-functionalized chiral Rh–diene complexes. Spiropyran has been reported to be pH responsive.<sup>55</sup> A neutral or basic corona can stabilize the photoresponsive shell and increase the responsiveness of the light trigger. The Rh-catalyzed asymmetric 1,4-addition reaction prefers neutral or basic conditions, and therefore, the corona of lithium carboxylic salts is a suitable nanodomain for the catalytic 1,4-addition.<sup>49,50</sup>

We synthesized the poly(2-oxazoline) triblock copolymers through CROP with methyl triflate as the initiator.<sup>57</sup> The polymerization process was monitored by <sup>1</sup>H NMR spectroscopy. After completion, the final triblock copolymer **1** was analyzed by <sup>1</sup>H NMR spectroscopy and gel-permeation chromatography (GPC) (for details, see the [Supporting Information](#)). The apparent molecular weight ( $M_n^{\text{app}}$ ) and dispersity ( $D$ ) were 5.4 kDa and 1.30, respectively. Hydrolysis of the ester block generated copolymer **2** with a carboxylate block (for details, see the [Supporting Information](#)). We dissolved copolymer **2** in water at 1.0 mg mL<sup>-1</sup> and characterized the self-assembled micelles by dynamic light scattering (DLS) ([Figure S17](#), left). No nanostructure formation was observed if the assembly was performed in an organic solvent such as methanol ([Figure S17](#), right). The micelles in water were cross-linked using copper(I)-catalyzed alkyne–azide cycloaddition (CuAAC) between the alkyne moiety and bifunctionalized spiropyran (N<sub>3</sub>-SP-N<sub>3</sub>) (see the [Supporting Information](#) for the synthesis and characterizations) to afford SCM **3**. The covalent cross-linking was confirmed by NMR and FT-IR spectroscopies by observing the disappearance of the characteristic alkyne signals at 1.98 ppm in the <sup>1</sup>H NMR spectrum, 84.7 and 71.0 ppm in the <sup>13</sup>C NMR spectrum, and 3278.6 cm<sup>-1</sup> in the FT-IR spectrum and the presence of the aromatic SP signals in the <sup>1</sup>H NMR spectrum, <sup>13</sup>C NMR spectrum, and IR spectrum ([Figures S18–S20](#)). The observation of the nanostructure via DLS after cross-linking and changing the solvent to methanol also indicated the successful covalent cross-linking of the micelles ([Figure S21](#)). A core–shell phase separated structure of the SCM domains was observed by cryogenic TEM (Cryo-TEM) imaging ([Figure 2a](#)).

Next, we investigated the photoresponsiveness of SCM **3** by DLS and Cryo-TEM. SCM **3** was dispersed in water at 0.5 mg/mL for DLS analysis and at 0.05 mg/mL for Cryo-TEM. The micelle solution was exposed to visible light ( $\lambda = 550$  nm) for 15 min and then switched to UV irradiation ( $\lambda = 350$  nm) for 15 min. The pink color of the micelle solution changed to dark purple while switching from visible to UV light. Once the first cycle was completed, the same UV/vis sequence was repeated for five consecutive UV/vis cycles. DLS measurements of SCM **3** showed hydrodynamic diameters ( $D_h$ ) under visible light of  $105 \pm 5$  nm. Upon irradiation with UV light, the  $D_h$  fluctuated between 58 and 70 nm, demonstrating a significant change in micelle morphology ([Figure 2b](#)). Similarly, reversible photo-switchability was observed when SCM **3** was dispersed in methanol accompanied by a color transition from dark yellow (under visible light) to dark red (under UV light) ([Figure](#)

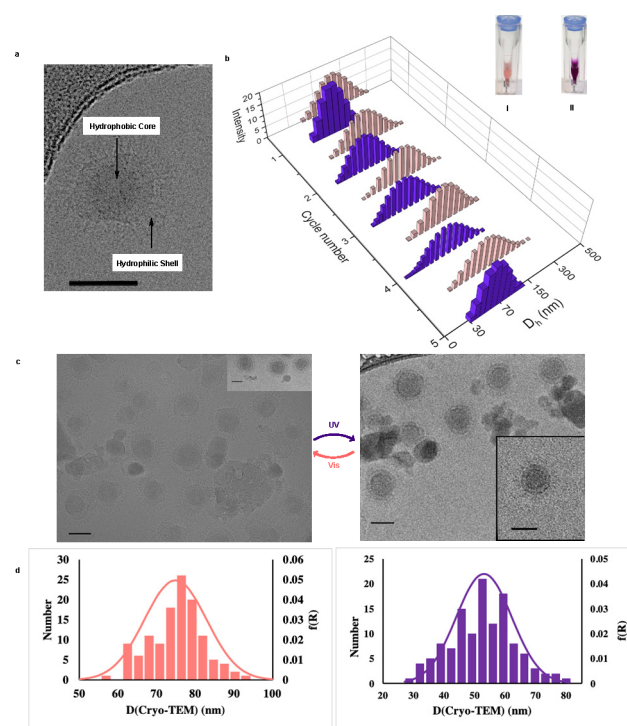
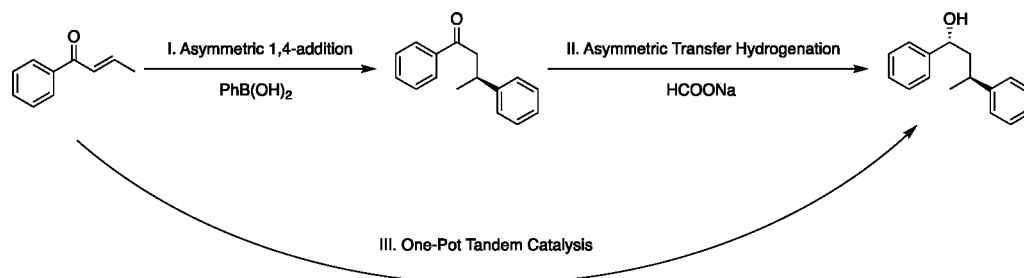


**Figure 2.** Morphological investigations of SCM **3**. (a) Cryo-TEM image of the phase separation of the SCM domains. A core–shell structure was observed. Scale bar = 50 nm. (b)  $D_h$  distributions of five consecutive cycles determined by DLS. The micelle solution turned pink after exposure to visible light for 15 min (I) and dark purple (II) after UV light irradiation for 15 min. (c) Cryo-TEM images of SCM **3** during visible light (left) and UV light (right) switching. Scale bar = 50 nm. (d) Statistical size distribution of SCM **3** under visible light (left) and UV-light (right) exposure based on 120 micelles from Cryo-TEM images.

[S21](#)). Statistical size distribution is based on a sample size of at least 120 micelles in the Cryo-TEM ([Figure 2c,d](#)). The  $z$ -average diameter for the micelles, calculated from the distribution, was 74 nm under visible light and 51 nm under UV irradiation. These results indicate that our smart SCMs have a photoinduced “breathing” feature.

With the photoswitchable SCM **3** in hand, the two chiral Rh catalysts were immobilized in two separate nanoenvironments via orthogonal chemistries. We first reacted the alkene functionalities in the core with a multivalent tetrathiol linker through thiol–ene click chemistry ([Scheme 1](#)). A ratio of 1:1 of alkene to tetradentate thiol linker was chosen, leaving an average of three free thiols per polymer chain for further functionalization with the alkene-functionalized Rh–TsDPEN through a second thiol–ene click addition to produce SCM **4**. A rhodium loading of 0.934% was determined by inductively coupled plasma-mass spectrometry (ICP-MS), corresponding to 1.63 Rh–TsDPEN catalysts per polymer chain for SCM **4**. After acidifying the corona domain, the hydroxy-functionalized Rh–diene complex was attached along the side-chains of the hydrophilic corona via *o*-(benzotriazol-1-yl)-*N,N,N',N'*-tetramethyluronium tetrafluoroborate (TBTU)/*N,N*-diisopropylethylamine (DIPEA)-mediated coupling. The corona domain of the resulting polymer was subsequently basified to obtain the final bifunctional SCM **5**. The rhodium content of the bifunctional SCM **5** was determined by ICP-MS to be 2.02%, corresponding to 1.86 Rh–diene complexes and 1.63

Table 1. Unsupported Catalytic Tests of Single- and Multistep Reactions



| entry <sup>a</sup> | transformation | catalyst             | cat. loading (mol %) | time (h) | conversion <sup>b</sup> (%) | ee <sup>c</sup> (%) | dr <sup>c</sup> (%) |
|--------------------|----------------|----------------------|----------------------|----------|-----------------------------|---------------------|---------------------|
| 1 <sup>d</sup>     | I              | Rh–diene             | 6                    | 15       | 99                          | 96                  |                     |
| 2 <sup>e</sup>     | I              | Rh–diene             | 6                    | 15       | 80                          | 96                  |                     |
| 3 <sup>e</sup>     | II             | Rh–TsDPEN            | 5                    | 20       | 72                          | 99                  | 96:4                |
| 4 <sup>d</sup>     | II             | Rh–TsDPEN            | 5                    | 20       | 15                          | nd                  | nd                  |
| 5 <sup>e</sup>     | III            | Rh–diene + Rh–TsDPEN | 6/5                  | 25       | 48 (47) <sup>f</sup>        | nd                  | nd                  |
| 6 <sup>d</sup>     | III            | Rh–diene + Rh–TsDPEN | 6/5                  | 25       | 73 (24) <sup>f</sup>        | nd                  | nd                  |

<sup>a</sup>Reaction conditions: all reactions were performed on a 0.02 mmol substrate scale in 3 mL of water at 40 °C. For transformation I, the reactions were performed with phenyl boronic acid (2.0 equiv) under an argon atmosphere. For transformation II, the reactions were performed with HCOONa (10 equiv) in open air. For transformation III, the reactions were performed with phenyl boronic acid (2.0 equiv) and HCOONa (10 equiv) under an argon atmosphere. <sup>b</sup>Conversions of final products for each transformation were determined by <sup>1</sup>H NMR spectroscopy using mesitylene as an internal standard. <sup>c</sup>Determined by chiral HPLC analyses. <sup>d</sup>KOH (0.5 equiv) was added to the reaction. <sup>e</sup>KOH was not added to the reaction. <sup>f</sup>The conversion in bracket is for (*R*)-1-phenylbutan-1-ol.

Table 2. Micelle-Supported Catalytic Tests of Single- and Multistep Reactions

| entry <sup>a</sup> | transformation | catalyst | cat. loading (mol %) | time (h) | conversion <sup>b</sup> (%) | ee <sup>c</sup> (%) | dr <sup>c</sup> (%) |
|--------------------|----------------|----------|----------------------|----------|-----------------------------|---------------------|---------------------|
| 1                  | I              | SCM 5    | 6                    | 15       | 99                          | 96                  |                     |
| 2                  | II             | SCM 4    | 5                    | 20       | trace                       |                     |                     |
| 3 <sup>d</sup>     | II             | SCM 4    | 5                    | 20       | 98                          | 99                  | 96:4                |
| 4                  | III            | SCM 5    | 6/5                  | 30       | 92                          | 99                  | 96:4                |
| 5 <sup>f</sup>     | III            | SCM 5    | 6/5                  | 30       | 90                          | 99                  | 96:4                |
| 6 <sup>f</sup>     | III            | SCM 5    | 6/5                  | 30       | 91 <sup>e</sup>             | 99                  | 96:4                |

<sup>a</sup>Reaction conditions: all reactions were performed on a 0.02 mmol substrate scale in 3 mL of water at 40 °C. (I) The reaction was performed with SCM 5 (9 mg, containing 1.3 μmol Rh–diene), phenyl boronic acid (2 equiv), and KOH (0.5 equiv) under an argon atmosphere. II: The reactions were performed with SCM 4 (9 mg, containing 1 μmol Rh–TsDPEN), HCOONa (10 equiv) in open air. III: The reactions were performed with SCM 5 (9 mg, containing 1.3 μmol of Rh–diene and 1 μmol of Rh–TsDPEN), phenyl boronic acid (2.0 equiv), KOH (0.5 equiv), and HCOONa (10 equiv) under an argon atmosphere. UV-light irradiation was applied after 15 h. <sup>b</sup>Conversions were determined by <sup>1</sup>H NMR spectroscopy using mesitylene as the internal standard. <sup>c</sup>Determined by Chiral HPLC analyses. <sup>d</sup>The reaction was performed under UV light irradiation. <sup>e</sup>The conversion was for the catalysis using recycled nanoreactors. <sup>f</sup>The tandem reaction was performed on a 50 mg (0.34 mmol) substrate scale in 50 mL of water and the conversion was based on the isolated product.

Rh–TsDPEN complexes per polymer chain. DLS of SCM 5 confirmed that the reversible photoswitchable behavior was retained after catalyst immobilizations (Figure S22).

Before using the micelle-supported catalytic system, we investigated the catalytic activity of both unsupported catalysts independently of each other and in the tandem transformation. In the presence of KOH (0.5 equiv), the unsupported Rh–diene catalyzed the asymmetric 1,4-addition of phenylboronic acids to *trans*-1-phenyl-2-buten-1-one quantitatively at 40 °C over 15 h with excellent enantioselectivities (96% ee) (Table 1, entry 1). Without the presence of KOH, the conversion dropped to 80% (96% ee) (Table 1, entry 2), which indicated that the addition of KOH enhances the catalytic activity to promote the Rh-catalyzed 1,4-addition.<sup>49</sup> Unsupported heterogeneous Rh–TsDPEN catalyzed the ATH of the hydrophobic and sterically hindered substrate (*S*)-1,3-diphenylbutan-1-one in water with 72% conversion over 20 h and excellent enantioselectivity (99% ee, 96:4 dr) (Table 1, entry 3). The enantioselectivity, activity, and recyclability of transition-metal complexes based on TsDPEN or its derivatives in the ATH

reaction are highly pH-dependent.<sup>51–53</sup> In the presence of KOH (0.5 equiv), the conversion of the ATH was only 15% (Table 1, entry 4), which is due to the basification of the reaction mixture (pH = 11.5) through the addition of KOH causing deactivation of the Rh–TsDPEN. Attempting the tandem reaction by combining the two catalysts without adding KOH resulted in 48% of (1*R*,3*S*)-1,3-diphenyl-1-butanol, the desired product from Pathway-1 and 47% of (*R*)-1-phenylbutan-1-ol, the side product from Pathway-2 (Figure 1a and Table 1, entry 5). This result confirmed the competitiveness of the two possible pathways (Figure 1a). Interestingly, in the presence of KOH (0.5 equiv), the tandem reaction yielded 73% of the desired (1*R*,3*S*)-1,3-diphenyl-1-butanol and 24% of (*R*)-1-phenylbutan-1-ol (Table 1, entry 6). The rationales behind the difference between entries 5 and 6 in Table 1 are as follows. (1) KOH facilitated the Rh-catalyzed 1,4-addition. As a result, more intermediate Ketone-1 was generated in entry 6, which resulted in a higher amount of (1*R*,3*S*)-1,3-diphenyl-1-butanol. (2) The mixture of phenyl boronic acid (p*K*<sub>a</sub> = 8.83) and KOH turned the reaction

slightly basic, which decreased the activity of the Rh-TsDPEN catalyst, compared to Table 1, entry 3. Entry 6 (Figure S37) of Table 1 shows the formation of multiple intermediates, the desired product and side products, during tandem catalysis confirmed the competitiveness between the two pathways. The unsupported catalytic tests of the single and tandem transformations demonstrated the incompatibility between two Rh catalysts and the existence of two competitive tandem reaction pathways. We reasoned that this tandem reaction presents a perfect testbed to investigate whether our strategy can circumvent catalyst incompatibility and photoregulate the reaction pathway to improve the overall synthetic efficiency.

We investigated the catalytic activity of the SCM for each single step transformation. SCM 5 catalyzed the asymmetric 1,4-addition of phenylboronic acids to *trans*-1-phenyl-2-buten-1-one quantitatively and with excellent enantioselectivities (96% ee) under the same conditions as the unsupported rhodium catalyst, which shows the hydrophilic corona is a suitable catalytic environment for this transformation (Table 2, entry 1). The ATH mediated with SCM 4 can be suppressed or accelerated according to the type of stimulus applied (Figure 3). Under visible light, the ATH with SCM 4 yielded

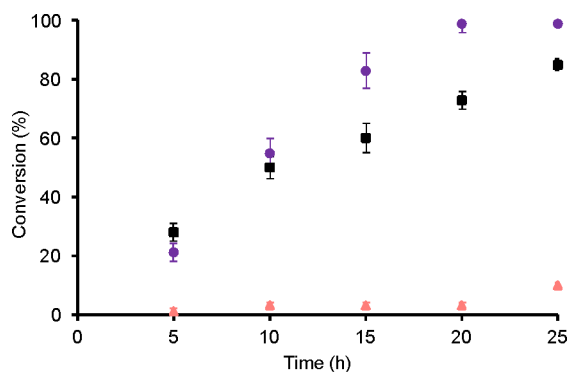


**Figure 3.** Conversion vs time for Table 1, entry 3, and Table 2, entries 2 and 3. Rh-TsDPEN-catalyzed ATH of (*S*)-1,3-diphenylbutan-1-one: purple circles represent the reaction with SCM 4 under UV light irradiation; black squares represent the reaction with unsupported Rh-TsDPEN; pink triangles represent the reaction SCM 4 under visible light. All reactions were performed on a 0.02 mmol substrate scale in 3 mL of water at 40 °C with 5 mol % Rh catalyst loading and HCOONa (10 equiv).

trace amounts of product in 20 h (Table 2, entry 3). Under UV irradiation, however, the ATH with SCM 4 was slightly accelerated in comparison to the unsupported Rh-TsDPEN catalyst with quantitative conversion and excellent enantioselectivities (99% ee, >96:4 dr) (Figure 3 and Table 2, entry 3). We hypothesize that under visible light the hydrophobic SP cross-linking layer prevents the diffusion of the hydrogen donor HCOONa into the core resulting in the suppression of the ATH. Under UV-light irradiation, the SP isomerizes to MC resulting in an increase in hydrophilicity of the cross-linking layer and ultimately an increase in permeability for HCOONa. The kinetic data (Figure 3) and the catalytic tests of the ATH (Table 2, entries 2 and 3) demonstrate that the phototriggered reversible spiropyran to merocyanine transition results in the gated behavior to SCMs, which is key to discriminating between substrates/reagents during catalysis; photomodulating the diffusion of HCOONa and providing an On/Off control over ATH catalysis.

Next, we investigated whether our smart SCM nanoreactors SCM 5 can facilitate two incompatible catalytic steps and photoregulate the reaction pathways. In the presence of KOH, SCM 5 catalyzed the asymmetric 1,4-addition of phenylboronic acids to *trans*-1-phenyl-2-buten-1-one to generate the only intermediate (*S*)-1,3-diphenylbutan-1-one (Ketone-1) (Figure 4). After 15 h, UV irradiation was applied resulting

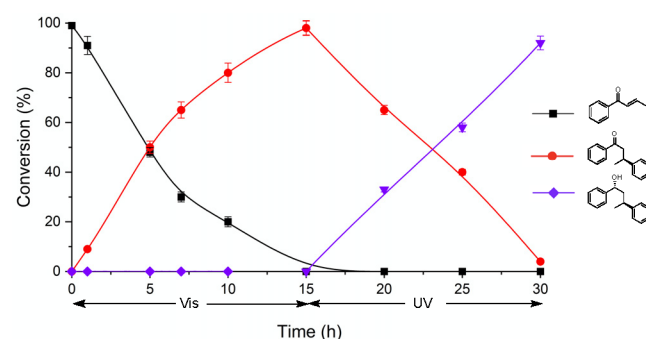


**Figure 4.** Time course of the tandem catalysis (Table 2, entry 4): Under visible light irradiation, SCM 5 catalyzed the asymmetric 1,4-addition of phenylboronic acids to *trans*-1-phenyl-2-buten-1-one to generate the only observed intermediate (*S*)-1,3-diphenylbutan-1-one accompanied by the complete consumption of starting material *trans*-1-phenyl-2-buten-1-one. After 15 h, UV irradiation was turned on to initiate the ATH to yield the desired and only product (*1R,3S*)-1,3-diphenyl-1-butanol (black squares, *trans*-1-phenyl-2-buten-1-one; red solid circles, (*S*)-1,3-diphenylbutan-1-one; purple rhombus, (*1R,3S*)-1,3-diphenyl-1-butanol; butyrophenone and (*R*)-1-phenylbutan-1-ol were not observed). Reaction conditions: 0.02 mmol of substrate scale in 3 mL of water at 40 °C with SCM 5 (9 mg, containing 1.3 μmol of Rh-Diene and 1 μmol of Rh-TsDPEN), phenyl boronic acid (2.0 equiv), KOH (0.5 equiv), and HCOONa (10 equiv) under an argon atmosphere and the UV irradiation was applied after 15 h.

in the activation of the ATH to yield the desired product (*1R,3S*)-1,3-diphenyl-1-butanol in 92% conversion with excellent enantioselectivities (99% ee, >96:4 dr) (Table 2, entries 4 and 5). These results indicated that the SCM 5 circumvented the incompatibility of the two catalysts via compartmentalization and that one reaction pathway can be selected over competing ones based on the external light stimulus (compare Table 2, entry 4, and Table 1, entries 5 and 6). The SCMs can be easily recovered via dialysis and recycled without major loss of reactivity (Table 2, entry 6).

A limited substrate screen was performed using SCM 5 (Table 3). Aromatic boronic acids, substituted with either electron-withdrawing or -donating groups, can be converted in high yields and ee and dr values (Table 3, entries 1–3). Aliphatic enone also underwent micellar tandem catalysis with high conversions (98%) and enantioselectivities (99% ee, 5:1 dr). In contrast, the unsupported one-pot tandem catalysis only yielded 48% desired product under the same reaction conditions (Table 3, entry 4).

## CONCLUSION

In summary, we realized the concept of compartmentalization and responsiveness with an artificial multicatalytic system that can photoregulate an efficient synthetic pathway for non-orthogonal tandem catalysis in water. The key design is a responsive cross-linking layer between the two compartments in a core-shell micellar nanostructure. The smart nanostructure responds to light irradiation in a wavelength-selective

Table 3. Substrate Scope for Micelle-Supported One-Pot Tandem Catalysis

| entry <sup>a</sup> | substrate | product | conversion (%) <sup>b</sup> | ee (%) <sup>c</sup> | dr (%) <sup>c</sup> |
|--------------------|-----------|---------|-----------------------------|---------------------|---------------------|
| 1                  |           |         | 92                          | 99                  | 98:2                |
| 2                  |           |         | 95                          | 96                  | 95:3                |
| 3                  |           |         | 85                          | 94                  | 97:3                |
| 4                  |           |         | 98 (48) <sup>d</sup>        | 99                  | 5:1                 |

<sup>a</sup>Reaction conditions unless otherwise indicated: SCM 5 (9 mg, containing 1.3  $\mu$ mol of Rh-Diene and 1  $\mu$ mol of Rh-TsDPEN), 0.02 mmol of enone (1.0 equiv), boronic acid (2.0 equiv), KOH (0.5 equiv), HCOONa (10 equiv) in 3 mL of water at 40 °C for 30 h under an argon atmosphere. UV-light irradiation was applied after 15 h. <sup>b</sup>Conversions were determined by <sup>1</sup>H NMR spectroscopy using mesitylene as an internal standard. <sup>c</sup>Determined by chiral HPLC analyses. <sup>d</sup>The conversion in parentheses was using unsupported catalysts under the same conditions.

manner. Two incompatible catalysts were spatially isolated in the hydrophilic corona and the hydrophobic core. The gated behavior induced by the phototriggered reversible spiropyran to merocyanine transition in the cross-linking layer is essential to discriminate among substrates/reagents during the catalysis. The smart SCM nanoreactor can circumvent incompatibility between the catalysts via compartmentalization and allows for the photoregulation of the desired reaction pathway. The smart SCM nanoreactors, on a basic level, mimic how cells use compartmentalization and responsiveness to coordinate thousands of incompatible chemical transformations into a streamlined metabolic process. Future research in our group will focus on preparing smart compartmentalized nanoreactors with more than two nanodomains and that can respond to multiple stimuli to regulate otherwise incompatible tandem reactions.

## ■ ASSOCIATED CONTENT

### Supporting Information

The Supporting Information is available free of charge at <https://pubs.acs.org/doi/10.1021/jacs.1c00257>.

Materials, synthetic procedures, characterizations of small molecules and macromolecules, and general procedures for micelle-supported single- and multistep catalysis (PDF)

## ■ AUTHOR INFORMATION

### Corresponding Author

Marcus Weck – Molecular Design Institute and Department of Chemistry, New York University, New York 10003, United States; [orcid.org/0000-0002-6486-4268](https://orcid.org/0000-0002-6486-4268); Email: [marcus.weck@nyu.edu](mailto:marcus.weck@nyu.edu)

## Authors

Peiyuan Qu – Molecular Design Institute and Department of Chemistry, New York University, New York 10003, United States

Michael Kuepfert – Molecular Design Institute and Department of Chemistry, New York University, New York 10003, United States

Maryam Hashmi – Molecular Design Institute and Department of Chemistry, New York University, New York 10003, United States

Complete contact information is available at: <https://pubs.acs.org/10.1021/jacs.1c00257>

## Notes

The authors declare no competing financial interest.

## ■ ACKNOWLEDGMENTS

Funding provided by the U.S. Department of Energy, Office of Basic Energy Sciences, through Catalysis Science Contract DE-FG02-03ER15459, is gratefully acknowledged. We thank Kristen Dancel-Manning from the OCS Microscopy Core and William J. Rice and Bing Wang from the Cryo-Electron Microscopy Laboratory at New York University Langone Medical Center for obtaining the Cryo-TEM images.

## ■ REFERENCES

- (1) Albrecht, L.; Jiang, H.; Jørgensen, K. A. A Simple Recipe for Sophisticated Cocktails: Organocatalytic One-Pot Reactions—Concept, Nomenclature, and Future Perspectives. *Angew. Chem., Int. Ed.* **2011**, *50*, 8492–8509.
- (2) Climent, M. J.; Corma, A.; Iborra, S.; Sabater, M. J. Heterogeneous Catalysis for Tandem Reactions. *ACS Catal.* **2014**, *4*, 870–891.
- (3) Lohr, T. L.; Marks, T. J. Orthogonal tandem catalysis. *Nat. Chem.* **2015**, *7*, 477–482.
- (4) Hayashi, Y. Pot economy and one-pot synthesis. *Chem. Sci.* **2016**, *7*, 866–880.

- (5) Kumar, G.; Nikolla, E.; Linic, S.; Medlin, J. W.; Janik, M. J. Multicomponent Catalysts: Limitations and Prospects. *ACS Catal.* **2018**, *8*, 3202–3208.
- (6) Li, L.; Herzon, S. B. Temporal separation of catalytic activities allows anti-Markovnikov reductive functionalization of terminal alkynes. *Nat. Chem.* **2014**, *6*, 22–27.
- (7) Agapakis, C. M.; Boyle, P. M.; Silver, P. A. Natural strategies for the spatial optimization of metabolism in synthetic biology. *Nat. Chem. Biol.* **2012**, *8*, 527–535.
- (8) Chen, A. H.; Silver, P. A. Designing biological compartmentalization. *Trends Cell Biol.* **2012**, *22*, 662–670.
- (9) Marguet, M.; Bonduelle, C.; Lecommandoux, S. Multi-compartmentalized polymeric systems: towards biomimetic cellular structure and function. *Chem. Soc. Rev.* **2013**, *42*, 512–529.
- (10) Mann, S. Systems of Creation: The Emergence of Life from Nonliving Matter. *Acc. Chem. Res.* **2012**, *45*, 2131–2141.
- (11) Buddingh', B. C.; van Hest, J. C. M. Artificial Cells: Synthetic Compartments with Life-like Functionality and Adaptivity. *Acc. Chem. Res.* **2017**, *50*, 769–777.
- (12) Gelman, F.; Blum, J.; Avnir, D. One-Pot Sequences of Reactions with Sol-Gel Entrapped Opposing Reagents: An Enzyme and Metal-Complex Catalysts. *J. Am. Chem. Soc.* **2002**, *124*, 14460–14463.
- (13) Yang, H.; Fu, L.; Wei, L.; Liang, J.; Binks, B. P. Compartmentalization of Incompatible Reagents within Pickering Emulsion Droplets for One-Pot Cascade Reactions. *J. Am. Chem. Soc.* **2015**, *137*, 1362–1371.
- (14) Ueda, Y.; Ito, H.; Fujita, D.; Fujita, M. Permeable Self-Assembled Molecular Containers for Catalyst Isolation Enabling Two-Step Cascade Reactions. *J. Am. Chem. Soc.* **2017**, *139*, 6090–6093.
- (15) Holloway, L. R.; Bogie, P. M.; Lyon, Y.; Ngai, C.; Miller, T. F.; Julian, R. R.; Hooley, R. J. Tandem Reactivity of a Self-Assembled Cage Catalyst with Endohedral Acid Groups. *J. Am. Chem. Soc.* **2018**, *140*, 8078–8081.
- (16) Moughton, A. O.; Hillmyer, M. A.; Lodge, T. P. Multicompartment Block Polymer Micelles. *Macromolecules* **2012**, *45*, 2–19.
- (17) Ahmed, E.; Womble, C. T.; Weck, M. Synthesis and Aqueous Self-Assembly of ABCD Bottlebrush Block Copolymers. *Macromolecules* **2020**, *53*, 9018–9025.
- (18) Womble, C. T.; Kuepfert, M.; Weck, M. Multicompartment Polymeric Nanoreactors for Non-Orthogonal Cascade Catalysis. *Macromol. Rapid Commun.* **2019**, *40*, 1800580.
- (19) Xie, G.; Zhang, J.; Ma, X. Compartmentalization of Multiple Catalysts into Outer and Inner Shells of Hollow Mesoporous Nanospheres for Heterogeneous Multi-Catalyzed/Multi-Component Asymmetric Organocascade. *ACS Catal.* **2019**, *9*, 9081–9086.
- (20) Isaacs, M. A.; Parlett, C. M. A.; Robinson, N.; Durdell, L. J.; Manayil, J. C.; Beaumont, S. K.; Jiang, S.; Hondow, N. S.; Lamb, A. C.; Jampaiah, D.; Johns, M. L.; Wilson, K.; Lee, A. F. A spatially orthogonal hierarchically porous acid–base catalyst for cascade and antagonistic reactions. *Nat. Catal.* **2020**, *3*, 960–931.
- (21) Quan, Y.; Lan, G.; Shi, W.; Xu, Z.; Fan, Y.; You, E.; Jiang, X.; Wang, C.; Lin, W. Metal–Organic Layers Hierarchically Integrate Three Synergistic Active Sites for Tandem Catalysis. *Angew. Chem., Int. Ed.* **2021**, *60*, 3115–3120.
- (22) Vázquez-González, M.; Wang, C.; Willner, I. Biocatalytic cascades operating on macromolecular scaffolds and in confined environments. *Nat. Catal.* **2020**, *3*, 256–273.
- (23) Zhou, K.; Tian, T.; Wang, C.; Zhao, H.; Gao, N.; Yin, H.; Wang, P.; Ravoo, B. J.; Li, G. Multifunctional Integrated Compartment Systems for Incompatible Cascade Reactions Based on Onion-Like Photonic Spheres. *J. Am. Chem. Soc.* **2020**, *142*, 20605–20615.
- (24) Liu, X.; Appelhans, D.; Voit, B. Hollow Capsules with Multiresponsive Valves for Controlled Enzymatic Reactions. *J. Am. Chem. Soc.* **2018**, *140*, 16106–16114.
- (25) Byard, S. J.; O'Brien, C. T.; Derry, M. J.; Williams, M.; Mykhaylyk, O. O.; Blanz, A.; Armes, S. P. Unique aqueous self-assembly behavior of a thermoresponsive diblock copolymer. *Chem. Sci.* **2020**, *11*, 396–402.
- (26) Yu, S.; Azzam, T.; Rouiller, I.; Eisenberg, A. Breathing<sup>®</sup> Vesicles. *J. Am. Chem. Soc.* **2009**, *131*, 10557–10566.
- (27) Wang, X.; Hu, J.; Liu, G.; Tian, J.; Wang, H.; Gong, M.; Liu, S. Reversibly Switching Bilayer Permeability and Release Modules of Photochromic Polymersomes Stabilized by Cooperative Noncovalent Interactions. *J. Am. Chem. Soc.* **2015**, *137*, 15262–15275.
- (28) Rifaie-Graham, O.; Ulrich, S.; Galensowske, N. F. B.; Balog, S.; Chami, M.; Rentsch, D.; Hemmer, J. R.; Read de Alaniz, J.; Boesel, L. F.; Bruns, N. Wavelength-Selective Light-Responsive DASA-Functionalized Polymersome Nanoreactors. *J. Am. Chem. Soc.* **2018**, *140*, 8027–8036.
- (29) Hu, J.; Zhang, G.; Liu, S. Enzyme-responsive polymeric assemblies, nanoparticles and hydrogels. *Chem. Soc. Rev.* **2012**, *41*, 5933–5949.
- (30) Randolph, L. M.; Chien, M.-P.; Gianneschi, N. C. Biological stimuli and biomolecules in the assembly and manipulation of nanoscale polymeric particles. *Chem. Sci.* **2012**, *3*, 1363–1380.
- (31) Wu, S.; Dzubiella, J.; Kaiser, J.; Drechsler, M.; Guo, X.; Ballauff, M.; Lu, Y. Thermosensitive Au-PNIPAA Yolk–Shell Nanoparticles with Tunable Selectivity for Catalysis. *Angew. Chem., Int. Ed.* **2012**, *51*, 2229–2233.
- (32) Lu, A.; Moatsou, D.; Hands-Portman, I.; Longbottom, D. A.; O'Reilly, R. K. Recyclable l-Proline Functional Nanoreactors with Temperature-Tuned Activity Based on Core–Shell Nanogels. *ACS Macro Lett.* **2014**, *3*, 1235–1239.
- (33) Blanco, V.; Leigh, D. A.; Marcos, V. Artificial switchable catalysts. *Chem. Soc. Rev.* **2015**, *44*, 5341–5370.
- (34) Kuepfert, M.; Qu, P.; Cohen, A.; Hoyt, C.; Jones, C.; Weck, M. Reversible Photoswitching in Poly(2-oxazoline) Nanoreactors. *Chem.—Eur. J.* **2020**, *26*, 11776–11781.
- (35) Renggli, K.; Baumann, P.; Langowska, K.; Onaca, O.; Bruns, N.; Meier, W. Selective and Responsive Nanoreactors. *Adv. Funct. Mater.* **2011**, *21*, 1241–1259.
- (36) Meng, J.; Chang, F.; Su, Y.; Liu, R.; Cheng, T.; Liu, G. Switchable Catalysts Used To Control Suzuki Cross-Coupling and Aza–Michael Addition/Asymmetric Transfer Hydrogenation Cascade Reactions. *ACS Catal.* **2019**, *9*, 8693–8701.
- (37) Li, X.; Sun, Y.; Wang, S.; Jia, X. Ru–Pd Thermoresponsive Nanocatalyst Based on a Poly(ionic liquid) for Highly Efficient and Selectively Catalyzed Suzuki Coupling and Asymmetric Transfer Hydrogenation in the Aqueous Phase. *ACS Appl. Mater. Interfaces* **2020**, *12*, 44094–44102.
- (38) Klermund, L.; Poschenrieder, S. T.; Castiglione, K. Biocatalysis in Polymersomes: Improving Multienzyme Cascades with Incompatible Reaction Steps by Compartmentalization. *ACS Catal.* **2017**, *7*, 3900–3904.
- (39) Vriezema, D. M.; Garcia, P. M. L.; Sancho Oltra, N.; Hatzakis, N. S.; Kuiper, S. M.; Nolte, R. J. M.; Rowan, A. E.; van Hest, J. C. M. Positional Assembly of Enzymes in Polymersome Nanoreactors for Cascade Reactions. *Angew. Chem., Int. Ed.* **2007**, *46*, 7378–7382.
- (40) Peters, R. J. R. W.; Marguet, M.; Marais, S.; Fraaije, M. W.; van Hest, J. C. M.; Lecommandoux, S. Cascade Reactions in Multi-compartmentalized Polymersomes. *Angew. Chem., Int. Ed.* **2014**, *53*, 146–150.
- (41) Helms, B.; Guillaudeu, S. J.; Xie, Y.; McMurdo, M.; Hawker, C. J.; Fréchet, J. M. J. One-Pot Reaction Cascades Using Star Polymers with Core-Confined Catalysts. *Angew. Chem., Int. Ed.* **2005**, *44*, 6384–6387.
- (42) Chi, Y.; Scroggins, S. T.; Fréchet, J. M. J. One-Pot Multi-Component Asymmetric Cascade Reactions Catalyzed by Soluble Star Polymers with Highly Branched Non-Interpenetrating Catalytic Cores. *J. Am. Chem. Soc.* **2008**, *130*, 6322–6323.
- (43) O'Reilly, R. K.; Hawker, C. J.; Wooley, K. L. Cross-linked block copolymer micelles: functional nanostructures of great potential and versatility. *Chem. Soc. Rev.* **2006**, *35*, 1068–1083.
- (44) Cotanda, P.; Lu, A.; Patterson, J. P.; Petzetakis, N.; O'Reilly, R. K. Functionalized Organocatalytic Nanoreactors: Hydrophobic

Pockets for Acylation Reactions in Water. *Macromolecules* **2012**, *45*, 2377–2384.

(45) Lu, J.; Dimroth, J.; Weck, M. Compartmentalization of Incompatible Catalytic Transformations for Tandem Catalysis. *J. Am. Chem. Soc.* **2015**, *137*, 12984–12989.

(46) Qu, P.; Kuepfert, M.; Jockusch, S.; Weck, M. Compartmentalized Nanoreactors for One-Pot Redox-Driven Transformations. *ACS Catal.* **2019**, *9*, 2701–2706.

(47) Lee, L.-C.; Lu, J.; Weck, M.; Jones, C. W. Acid–Base Bifunctional Shell Cross-Linked Micelle Nanoreactor for One-Pot Tandem Reaction. *ACS Catal.* **2016**, *6*, 784–787.

(48) Kuepfert, M.; Cohen, A. E.; Cullen, O.; Weck, M. Shell Cross-Linked Micelles as Nanoreactors for Enantioselective Three-Step Tandem Catalysis. *Chem. - Eur. J.* **2018**, *24*, 18648–18652.

(49) Hayashi, T.; Takahashi, M.; Takaya, Y.; Ogasawara, M. Catalytic Cycle of Rhodium-Catalyzed Asymmetric 1,4-Addition of Organoboronic Acids. Arylrhodium, Oxa- $\pi$ -allylrhodium, and Hydrox- $\sigma$ -allylrhodium Intermediates. *J. Am. Chem. Soc.* **2002**, *124*, 5052–5058.

(50) Shen, G.; Osako, T.; Nagaosa, M.; Uozumi, Y. Aqueous Asymmetric 1,4-Addition of Arylboronic Acids to Enones Catalyzed by an Amphiphilic Resin-Supported Chiral Diene Rhodium Complex under Batch and Continuous-Flow Conditions. *J. Org. Chem.* **2018**, *83*, 7380–7387.

(51) Wu, X.; Liu, J.; Di Tommaso, D.; Iggo, J. A.; Catlow, C. R. A.; Bacsá, J.; Xiao, J. A Multilateral Mechanistic Study into Asymmetric Transfer Hydrogenation in Water. *Chem. - Eur. J.* **2008**, *14*, 7699–7715.

(52) Dimroth, J.; Keilitz, J.; Schedler, U.; Schomäcker, R.; Haag, R. Immobilization of a Modified Tethered Rhodium(III)-*p*-Toluenesulfonyl-1,2-diphenylethylenediamine Catalyst on Soluble and Solid Polymeric Supports and Successful Application to Asymmetric Transfer Hydrogenation of Ketones. *Adv. Synth. Catal.* **2010**, *352*, 2497–2506.

(53) Dimroth, J.; Schedler, U.; Keilitz, J.; Haag, R.; Schomäcker, R. New Polymer-Supported Catalysts for the Asymmetric Transfer Hydrogenation of Acetophenone in Water – Kinetic and Mechanistic Investigations. *Adv. Synth. Catal.* **2011**, *353*, 1335–1344.

(54) Klajn, R. Spiropyran-based dynamic materials. *Chem. Soc. Rev.* **2014**, *43*, 148–184.

(55) Kortekaas, L.; Browne, W. R. The evolution of spiropyran: fundamentals and progress of an extraordinarily versatile photochrome. *Chem. Soc. Rev.* **2019**, *48*, 3406–3424.

(56) Verbraeken, B.; Monnery, B. D.; Lava, K.; Hoogenboom, R. The chemistry of poly(2-oxazoline)s. *Eur. Polym. J.* **2017**, *88*, 451–469.

(57) Glassner, M.; Vergaelen, M.; Hoogenboom, R. Poly(2-oxazoline)s: A comprehensive overview of polymer structures and their physical properties. *Polym. Int.* **2018**, *67*, 32–45.

(58) Lava, K.; Verbraeken, B.; Hoogenboom, R. Poly(2-oxazoline)s and click chemistry: A versatile toolbox toward multi-functional polymers. *Eur. Polym. J.* **2015**, *65*, 98–111.